Technological aspects of growth and optical properties of thin CIGS films

P. P. Horley[*, **], Y. V. Vorobiev
[*]*Unidad Querétaro del CINVESTAV-IPN*
Querétaro, QRO, México

V. V. Khomyak, V. V. Gorley, S. V. Bilichuk,
[**] *Department of Physical Electronics and Non-Traditional Energy Sources,*
Chernivtsi National University, Chernivtsi, Ukraine

J. González-Hernández
CIMAV
Miguel de Cervantes 120, Chihuahua 31109, México
(Recibido 4 de octubre de 2003; Aceptado 23 de agosto de 2004)

The paper discusses the results of structural and optical investigations of $CuIn_xGa_{1-x}Se_2$ (CIGS) semiconductor films with molar composition $0 \le x \le 1$ obtained by thermal evaporation in vacuum. Experimental methods used to characterize the materials included ellipsometry measurements in the 250-800 nm wavelength range and X-ray structural analysis, which proved the polycrystalline nature of the films with chalcopyrite structure and a preferred direction (112). Surface investigation performed with SEM and AFM reported rough character of the film surface. Spectral dependence of real and imaginary parts of dielectric constant was investigated using Kramers-Kronig relation. It was shown that for the spectral range $\lambda < 0.5 \mu m$, the dielectric components of $CuIn_{0.2}Ga_{0.8}Se_2$ do not obey the principle of causality, which could be a consequence of light scattering peculiarities over statistically uneven film surface. The position of energy levels of the valence band of $CuIn_{0.2}Ga_{0.8}Se_2$ was estimated for the wavelengths $0.50 < \lambda < 0.84 \mu m$.

Keywords: Chalcopyrite semiconductors; CIGS; Sputtering; Thin films; Ellipsometry; Dielectric constant; Kramers-Kronig relation; Band structure.

1. Introduction

Complex ternary semiconductor $A^IB^{III}C_2^{VI}$ compounds and solid solutions based on them are intensively investigated nowadays as materials showing significant potential for photo-voltaic applications. This is caused by the peculiar band structure of the material, leading to specific electrical and optical properties [1]. Solar cells based on $A^IB^{III}C_2^{VI}$ semiconductors, developed by implementing modern achievements of material science, are capable to gain efficiency up to 18.8% [2,3]. Among the materials of this group, $CuIn_xGa_{1-x}Se_2$ (CIGS) is the most studied one, from both technological and device manufacturing points of view. As it follows from numerous structural, optical and photoelectric data obtained for $CuIn_xGa_{1-x}Se_2$ films, they are mainly polycrystalline with chalcopyrite structure [4-6], featuring grain size 0.2-2μm depending on synthesis technology [4,5]. Complex band structure of CIGS observed experimentally was explained by tetragonal lattice distortion and hybridization of copper d-levels with p-levels of chalcogene in the valence band [7,8]. Despite such detailed characterization of the material, published data on CIGS optical and photoelectric properties are quite controversial (e.g. [9-12]). It is caused mainly by limitations of common methodology to obtain the data on optical properties from transmission and reflection spectra only. This approach is treats the system as an infinite flat absorptive film deposited over transparent substrate [13,14,15,9-12], while the influence of film surface on photoelectric properties of the material is usually neglected. In the same time it is well known that rough surface structure leads to reflection peculiarities, such as admixture of diffused light component to the reflected one [16]. If the mean quadratic height of the surface formations δ is comparable or less than the wavelength of incident light λ, the effect of diffraction has to be also considered [17].

CIGS experimental data reported in scientific literature

Table 1. $CuIn_xGa_{1-x}Se_2$ films deposition conditions depending on composition x.

Sample #	x	T_E, (ºC)	T_S, (ºC)	**t,** (min)	**d,** (μm)
20	0.0	1300	400	30	1.3
13	0.2	1150	350	45	0.2
15	0.2	1200	350	120	0.9
17	0.5	1200	300	20	0.5
18	0.5	1200	350	30	0.5
19	1.0	1100	300	20	0.3

Table 2. Valence band parameters of $CuIn_{0.2}Ga_{0.8}Se_2$ thin films.

Transition	Data [5]	Our data	% of difference between our data and data from [5]
	Transition energy, eV		
$E_A = \Gamma_7^v \rightarrow \Gamma_6^c$	1.48	–	–
$E_B = \Gamma_6^v \rightarrow \Gamma_6^c$	1.57	1.54	1.9
$E_C = \Gamma_7^v \rightarrow \Gamma_6^c$	(1.74?)	1.65	–
E_D	(1.74?)	1.75	0.6
E_E	–	1.88	–
E_F	1.99	2.00	0.5
E_G	2.09	2.11	1.0
E_H	2.21	2.22	0.5

were obtained mainly for the wavelengths 0.4 – 2μm [15, 12], measured for the samples with grain size of δ≤ 0.5μm [4, 5]. Therefore, δ/λ relation for the data published is about unity; it becomes quite expectable [16] that the presence of diffused light component together with diffraction could influence the reflection properties of the material. This may lead to changes in the optical characteristics. As far as we know, the influence of rough surface on the optical properties of CIGS was generally neglected and lacks detailed investigation. This paper is dedicated to partial solution of this problem using ellipsometry data [17,18], making some comments on $CuIn_xGa_{1-x}Se_2$ growth technology and presents X-ray, SEM and AFM investigation results of the materials. The analysis of real and imaginary components of dielectric constant was performed using Kramers-Kronig relation [19]. Additionally, the position of valence band energy levels of CIGS was estimated for Γ-point of the Brillouin zone in the frame of quasi-cubic model [20].

2. Experimental

2.1. Preparation of CIGS crystal and thin films

Bulk crystals of CIGS were obtained using bi-temperature synthesis with further crystallization under radial temperature gradient, which improves the melt mixing because of convection [21]. To ensure high quality of the ingots, we have used initial elements (Cu, In, Ga, Se) with purity level 5N. Quartz tube with Cu, In and Ga in stoichiometric proportion plus Se in excess quantity was sealed in vacuum and inserted horizontally into bi-chamber oven. The temperature of the high-temperature chamber was about 1100-1200°C, while the low-temperature one was kept at 700-800°C depending on the molar composition of CIGS required. Programmable changes of chamber temperature by optimized temporal pattern made it possible to take advantage of controlled crystallization under high-pressure of Se vapors. CIGS monocrystals grown in this way were up to 10 mm in diameter and about 30 mm long, without macroscopic structural defects such as cavities or cracks. X-ray diffraction was used for advanced structure analysis of the samples; their level of stoichiometry was investigated with micro-phase analysis.

Thin films of CIGS were deposited by sputtering in vacuum (1×10^{-5} Torr) using $CuIn_xGa_{1-x}Se_2$ powder, obtained from the ingots of required composition by grinding and milling. To determine the dependence of film properties on substrate type we used both glass and silicon substrates. Thermal evaporation was performed with vacuum equipment VUP-5. Evaporator temperature was 1150–1300ºC for all the deposition process. The distance between the substrate and evaporator was 8 cm; the temperature of the substrate was kept at 300–400°C. Before the deposition of the film, the substrate was cleaned with ammoniac-peroxide, rinsed in distilled water, and dried in air.

2.2 Characterization of CIGS films

The estimation of the film thickness *d* was done with Linnik interferometer MII-4 with subsequent correction using optical polarization methods on UNIVEL/DH10 (240–830nm) equipment with Glan-Taylor polarizer and analyzer. The values of thickness were in the range 0.2 - 1.3μm depending on deposition time *t*, temperatures of the substrate T_S and evaporator T_E.

If the values of T_S and T_E were fixed, the thickness of the film was controlled by deposition time ranging from 20 to 120min. (see Table 1). The composition and structural analysis of the films was performed with X-ray diffraction analysis; surface quality and grain sizes were estimated from SEM and AFM investigations.

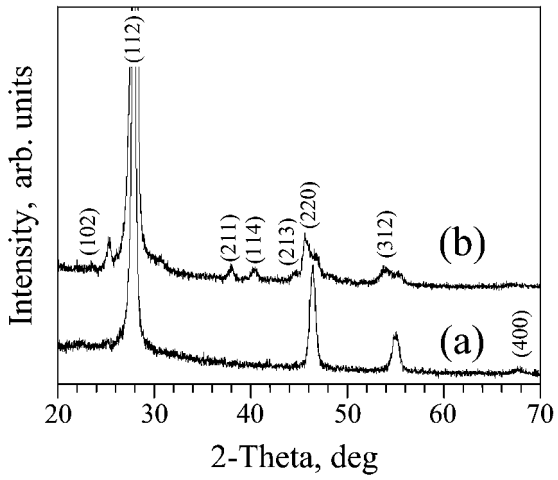

Figure 1. X-ray diagrams of $CuIn_{0.2}Ga_{0.8}Se_2$ sample #13 (a) and sample #15 (b).

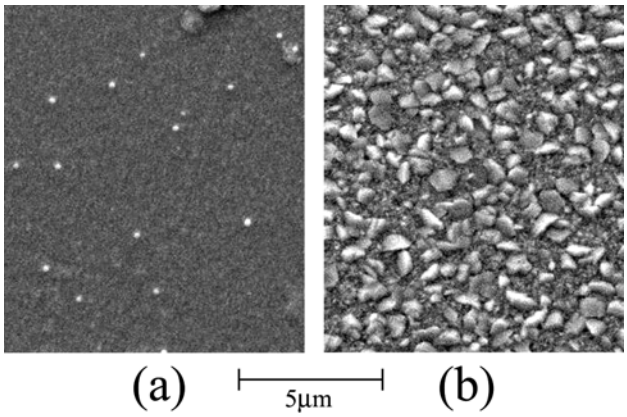

Figure 2. SEM images of CIGS film surface, sample #13 (a) and sample #15 (b).

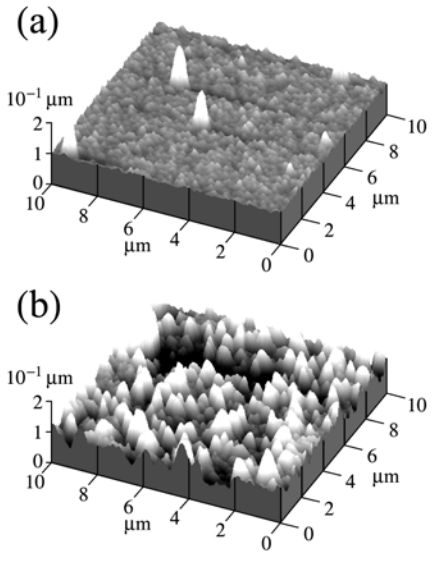

Figure 3. Surface morphology obtained with Atomic Force Microscopy: (a) sample #13, (b) sample #15.

3. Results and Discussion

All the samples described in Table 1 were subjected to detailed investigations as described above. In this paper, the authors present the data obtained for $CuIn_{0.2}Ga_{0.8}Se_2$ films (samples #13 and #15) to focus attention on the influence of surface roughness on real part of CIGS dielectric constant. We will consider the dependence of film parameters over its molar composition in a separate paper.

X-ray diffraction patterns of the samples considered are shown in Fig. 1. All major peaks correspond to $CuIn(Ga)Se_2$. The relative peak intensity reveals preferred orientation (112) which is better pronounced for the sample #15, for which other characteristic peaks (220) and (312) are significantly smaller and blurry. Faint chalcopyrite $CuInSe_2$ peak (211) and clear K_α line corresponding to the main peak (112) are absent in the case of sample #13. Both SEM (Fig. 2) and AFM (Fig.3) images confirm that the surface of sample #13 is more even and fine-grained ($\delta \sim$ 0.1-0.2μm) than that of sample #15, which has rough granular structure with average grain size of 0.7-0.8μm. Both samples are polycrystalline, with structurally uniform surface without discontinuities or cracks. Other samples mentioned in Table 1 featured grains of 0.5-2μm in size depending on substrate type and conditions during the film deposition.

The components of complex dielectric constant $\varepsilon = \varepsilon_1 + i\varepsilon_2$ determine optical properties of the material. They must obey the principle of causality [22], which is given through Kramers-Kronig dispersion relation [21]:

$$\varepsilon_1(\omega) - \varepsilon_1(\infty) = \frac{2}{\pi} P\int_0^\infty \frac{\omega' \varepsilon_2(\omega')}{\omega'^2 - \omega^2} d\omega', \qquad (1)$$

where P is the main value of the integral and $\varepsilon_1(\infty)$ is real component of high-frequency dielectric constant. In the limit case $\omega \to 0$ expression (1) transforms to the sum rule in a form characteristic for semiconductors.

$$\varepsilon_1(0) - \varepsilon_1(\infty) = \frac{2}{\pi} P\int_0^\infty \frac{\varepsilon_2(\omega')}{\omega'} d\omega'. \qquad (2)$$

It is important that (1) defines $\varepsilon_1(\omega)$ without any controversy with physical sense, even for the case when $\varepsilon_2(\omega) > 0$ for $\omega > 0$.

Spectral dependence of $\varepsilon_1(\omega)$ and $\varepsilon_2(\omega)$ obtained from ellipsometric measurements is shown in Fig.4, curves 1 and 2 respectively. As one can see, for the range $1.5 < \hbar\omega < 2.14$ eV the dependence of $\varepsilon_1(\omega)$ is in the same phase with $\varepsilon_2(\omega)$ (i.e. obeys Kramers-Kronig relation), but for $\hbar\omega > 2.14$ eV they lost synchronicity and

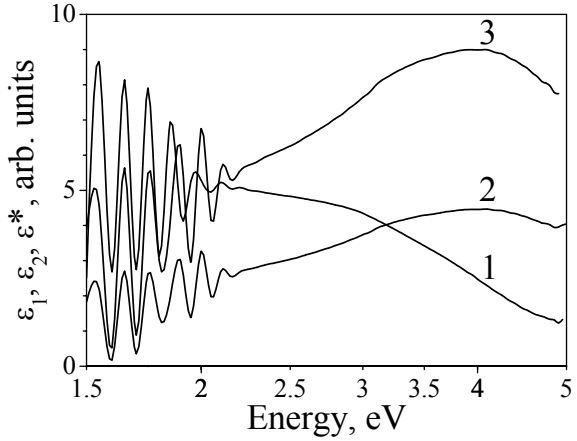

Figure 4. Dependence of dielectric constant components ε_1 and ε_2 obtained from ellipsometry measurements (curves 1 and 2) and theoretical dependence of ε* on incident quantum energy (curve 3).

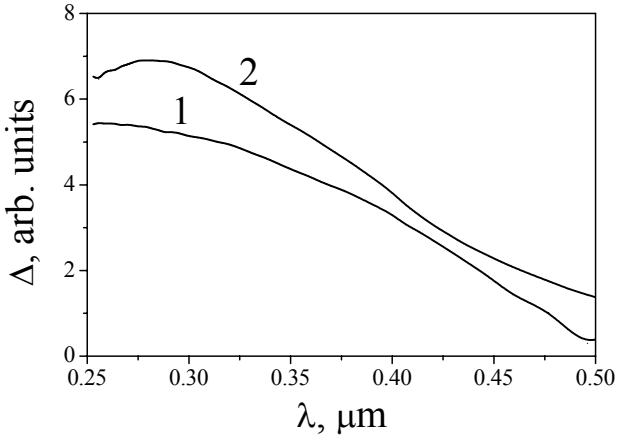

Figure 5. Dependence of $\Delta=\varepsilon^* - \varepsilon_1$ on wavelength of incident light: 1 – sample #13, 2 – sample #15.

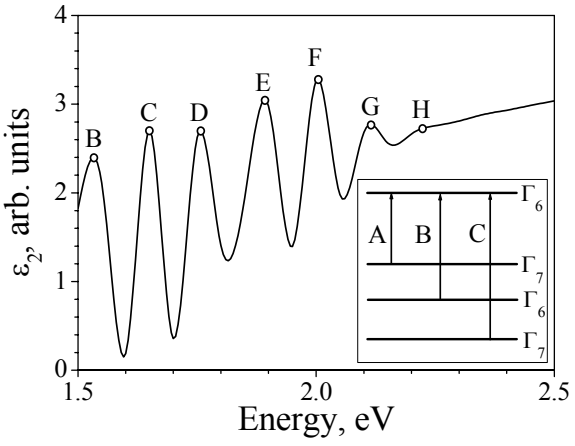

Figure 6. Determination of energies corresponding to transitions from different sub-bands of CIGS valence band. On the inset: the scheme of valence band structure considered.

do not satisfy (1) anymore. The difference between $\varepsilon_1(\omega)$ and $\varepsilon_2(\omega)$ for $\hbar\omega > 2.14$ eV is caused by the lack of information to describe the system properly, if one gets the data using the standard models [27,18] from phase difference Δ and relative amplitude change φ, measured experimentally. Indeed, as it is seen from Fig. 2, both samples feature structured surface with different grain size depending on the conditions during the film growth. Considering this, we suppose that the phase difference between $\varepsilon_1(\omega)$ and $\varepsilon_2(\omega)$ for $\hbar\omega > 2.14$ eV could be attributed to additional light scattering over statistically uneven surface, which is neglected in the standard model. To make a qualitative estimation of the surface influence, we have calculated numerically spectral dependence of $\varepsilon_1^c(\omega) \equiv \varepsilon^*$ (Fig. 4, curve 3) obeying the causality requirements (1). Fig. 5 shows spectral dependence of the difference $\Delta = \varepsilon_1(\lambda) - \varepsilon^*(\lambda)$ for the samples #13 (curve 1) and #15 (curve 2). Both of them are the curves with a maximum at the wavelength λ_m, which shows correlation with surface grain size. In particular, $\lambda_m \approx 0.28$ μm corresponds to the sample #15 with grain size of 0.7-0.8μm, while sample #13 with grains of 0.1-0.2μm is characterized with $\lambda_m < 0.25$ μm.

We consider that the correlation proves that the structure of the film surface has a strong influence on its optical parameters and has to be considered in corresponding theoretical models to ensure correct interpretation of experimental data.

As experimental dependence of $\varepsilon_1(\omega)$ and $\varepsilon_2(\omega)$ is synchronous in energy interval $1.5 < \hbar\omega < 2.14$ eV (Fig. 4), it could be used to determine the location of critical points in Brillouin zone of CIGS film because the energy, corresponding to the position of the maximum of $\varepsilon_2(h\nu)$ curve (Fig. 6) is defined with the sum of inter-band density of states [6]. The band diagram of $A^IB^{III}C_2^{VI}$ compounds features the valence band of a complex structure, with 16 branches grouped into several sub-bands divided with local energy gaps [1]. The top of the valence band is located in the point Γ of Brillouin zone, with upper sub-bands corresponding to Γ_6 and Γ_7 representations (inset to Fig.6). Valence band parameters of $CuIn_{0.2}Ga_{0.8}Se_2$ thin films presented in Table 2 were determined from Fig. 6 for the model of Hopfield [20], when valence band splitting of $A^IB^{III}C_2^{VI}$ materials is attributed to tetragonal field of the crystal lattice and spin-orbital interaction (e.g., [1,23,13,14,20]).

As it follows from the Table 2, the deviation of the data obtained with those from [5] is quite acceptable and does not surpass 2%. In our case, E_A transition corresponding to low-energy valence sub-bands was not observed because of wavelength range limitation of the equipment. In addition to the levels 1.54, 1.75, 2.00, 2.11, and 2.22 eV [5,11] we have detected two new ones with energies of 1.65 and 1.88

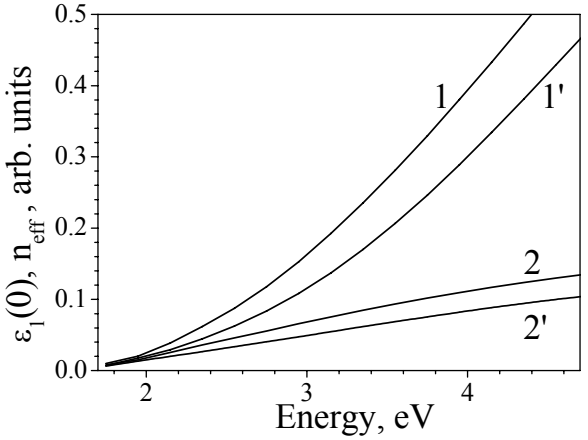

Figure 7. Calculated dependence of $\varepsilon_1(0)$ component increase (curves 1, 1') and effective number of valence electrons per atom n_{eff} (curve 2, 2') on incident light energy. Curves 1,2 correspond to the sample #13, curves 1', 2'– to the sample #15.

eV. The nature of these levels as well as type of corresponding transitions requires further investigations. The real component of dielectric constant could be used to determine the increase of static dielectric constant $\varepsilon_1(0)$ from the shift of $\varepsilon_2(\omega)$ towards lower energies. Dependence of $\varepsilon_1(0)$, obtained from numerical calculations of integral (2) in the range of 1.5 – 5.0 eV, is presented in Fig. 7. Curve 1 and 1' corresponds to the samples #13 and #15 respectively. As one can see, the shift of $\varepsilon_2(\omega)$ leads to greater $\varepsilon_1(0)$ for the film with smaller grains, because it has higher optical homogeneity in comparison with sample #15. However, $\varepsilon_1(0)-\varepsilon_1(\infty)>1$ in the case of semiconductor material; as it follows from our data, high-energy levels of the valence band are important for determination of $\varepsilon_1(\omega)$ and $\varepsilon_2(\omega)$. It is probable that energy levels of conduction band must be considered too. The latter could be verified calculating effective number of valence electrons per atom according to [24]:

$$n_{eff} \equiv n \cdot \frac{2\pi^2 e^2 \hbar^2 N_0}{m} = \frac{\hbar^2}{E_{\min}^2} \cdot \int_{E_{\min}}^{E_{\max}} \omega \varepsilon_2(\omega) d\omega , \qquad (3)$$

where N_0 is a density of atoms in the crystal, m is the mass of the electron and energy range in question is limited with E_{min} and E_{max}. Again, for film with smaller grains (Fig.7, curve 2), n_{eff} increases with higher rate that that corresponding to the sample #15 (Fig. 7, curve 2'). The most important feature of Fig. 7 is the absence of saturation of either $n_{eff}(\omega)$ and $\varepsilon_1(0)$. This means that high-energy levels of both valence and conductivity bands has to be considered for correct definition of optical characteristics of CIGS material.

4. Conclusions

The complex investigations of $CuIn_xGa_{1-x}Se_2$ thin films, obtained by sputtering, have shown strong influence of surface structure of the film on its optical properties. From the analysis of ellipsometry data, it follows that film grain size has to be taken into account to determine correct values of complex dielectric constant ε. This fact was verified by existence of correlation between grain size and degree of increase of both dielectric constant and efficient number of valence electrons per atom. It was also shown that high-energy levels must be considered for correct processing of CIGS optical characteristics.

References

[1] J.L. Shay and J.H., Wernick. Pergamon Press, New York (1975)
[2] M.A. Contreras, B. Egaas, J. Hiltner, A. Zwartzlander, F. Hasoon, R. Nuoffi, Progr. Photovolt.:Res.Appl. **7,** 311 (1999).
[3] L. Stolt, J. Hodstrom, J.Kesslitz, M. Ruch, K.-o. Velthaus, H.W. Schook, Appl. Phys.Lett. **62**, 597 (1993).
[4] T. Nakada, K. Migita, and A. Kunioka, Jpn. J. Appl. Phys **32**, 1169 (1993).
[5] Y. Sudo, S. Endo, and T. Irie, Jpn. J. Appl. Phys. **32**, 1562 (1993).
[6] S.J. Fonash, Solar Cell Device Physics, Academic Press, New York (1981).
[7] J.L. Shay, B. Tell, H.M. Kasper, and L.M. Schiavone, Phys. Rev. **B5**:12, 5003 (1972).
[8] J.L. Shay and H.M. Kasper, Phys. Rev. Lett. **29**, 1162 (1972).
[9] A.S. Kindyak, V.V. Kindyak, and Yu.V. Rud, Fizika i Tehnika Poluprovodnikov. (*in Russian*) **31**, 1033 (1997).
[10] T. Yamaguchi, J. Matsufusa, and A. Yoshida, Jpn. J. Appl. Phys. **31**, 603 (1992).
[11] A. Zegadi, M.A. Slifkin, M. Diamin, A.E. Hill, and R.D. Tomlinson, Phys. Stat. Sol. **13**, 533 (1992).
[12] J.R. Tuttle, D. Albin, R.J. Matson, and R. Noufi, J. Appl. Phys. **66**, 4408 (1989).
[13] V.V. Kindyak, A.S. Kindyak, V.F. Gremenok, I.V. Bodnar, Yu.V. Rud, and G.A. Medvedkin, Fizika i Tehnika Poluprovodnikov (in Russian) **27**, 1154 (1993).
[14] V.F. Gremenok, V.V. Nindyak, E.P. Zaretskaya, A.S. Kindyak, I.A. Viktorov, I.V. Bodnar, and Yu.V. Rud., Fizika i Tehnika Poluprovodnikov **29**, 1692 (1995).
[15] T. Yamaguchi, J. Matsufusa, and A. Yoshida, *Optical Transitions in RF Sputtered $CuIn_xGa_{1-x}Se_2$ Thin Films*, Jpn. J. Appl. Phys. **31**, **L**703 (1992).
[16] F.G. Bass and I.M. Fuks, Nauka, Moscow (1972).
[17] M.M. Gorshkov, Ellipsometry, Sovetskoe Radio, Moscow (1974) (in Russian)
[18] P.S. Hauge, Surf. Sci.**96**, 108 (1980).
[19] H.M. Nussenzveig, Academic Press, New York (1972).
[20] J.E. Rowe and J.L. Shay, Phys. Rev. B. **3**, 451 (1971).
[21] J. Gonzalez Hernandez, Yu.V. Vorobiev, P.P. Horley, P.N. Gorley, V.V. Khomyak, A.I. Savchuk, Z.D. Kovalyuk, and O.N. Sydor, Abstracts of E-MRS 2003 Spring Meeting, Strasbourg, France O/P11.25 (2003).
[22] F. Stern, Solid State Physics **15**, 300 (1963).
[23] V.Yu Rud and Yu.V. Rud, Fizika i Tehnika Poluprovodnikov (in Russian) **33**, 954 (1999).
[24] H.R. Philipp, H. Ehrenreich, Phys Rev. **129**, 1550 (1963).